DTIC COPY

REPORT DOCUMENTATION PAGE

Form Approved
OMB No. 0704-01-0188

PLEASE DO NOT RETURN YOUR FORM TO THE ABOVE ADDRESS.

1. REPORT DATE (DD-MM-YYYY)	2. REPORT TYPE	3. DATES COVERED (From - To)
10-06-2008	REPRINT	

4. TITLE AND SUBTITLE

On the R-dependence of the spin-orbit coupling constant: Potential energy functions of Xe_2^+ by high-resolution photoelectron spectroscopy and *ab initio* quantum chemistry

5a. CONTRACT NUMBER

5b. GRANT NUMBER

5c. PROGRAM ELEMENT NUMBER
61102F

6. AUTHORS
O. Zehnder*
R. Mastalerz*
M. Reiher*
F. Merkt*
R.A. Dressler

5d. PROJECT NUMBER
2303

5e. TASK NUMBER
RS

5f. WORK UNIT NUMBER
A1

7. PERFORMING ORGANIZATION NAME(S) AND ADDRESS(ES)

Air Force Research Laboratory /RVBXR
29 Randolph Road
Hanscom AFB, MA 01731-3010

8. PERFORMING ORGANIZATION REPORT NUMBER
AFRL-RV-HA-TR-2008-1053

9. SPONSORING/MONITORING AGENCY NAME(S) AND ADDRESS(ES)

10. SPONSOR/MONITOR'S ACRONYM(S)
AFRL/RVBXR

11. SPONSOR/MONITOR'S REPORT NUMBER(S)

12. DISTRIBUTION/AVAILABILITY STATEMENT
Approved for Public Release; distribution unlimited.

13. SUPPLEMENTARY NOTES
Reprinted from *Journal of Chemical Physics,* Vol. 128, 234306 (2008) doi:10.1063/1.2937133]
*Laboratorium fur Physikalische Chemie, ETH Zurich, 8093 Zurich, Switzerland

14. ABSTRACT

The pulsed-field ionization zero-kinetic-energy photoelectron spectrum of Xe_2 has been measured between 97,350 and 108,200 cm^{-1}, following resonant two-photon excitation via selected vibrational levels of the C 0_u^+ Rydberg state of Xe. Transitions to three of the six low-lying electronic states of Xe_2^+ could be observed. Whereas extensive vibrational progressions were observed for the transitions to the I(3/2*g*) and I(3/2*u*) states, only the lowest vibrational levels of the II(1/2*u*) state could be detected. Assignments of the vibrational quantum numbers were derived from the analysis of the isotopic shifts and from the modeling of the potential energy curves. Adiabatic ionization energies, dissociation energies, and vibrational constants are reported for the I(3/2*g*) and the I(3/2*u*) states. Multireference configurational interaction and complete active space self-consistent field calculations have been performed to investigate the dependence of the spin-orbit coupling constant on the internuclear distance. The energies of vibrational levels, measured presently and in a previous investigation (Rupper *et al.*, J. Chem. Phys. **121**, 8279 (2004)), were used to determine the potential energy functions of the six low-lying electronic states of Xe_2^+ using a global model that includes the long-range interaction and treats, for the first time, the spin-orbit interaction as dependent on the internuclear separation.

15. SUBJECT TERMS

Pulsed-field ionization Xenon dimer ion Photoelectron spectrum Resonant two-photon excitation
Spin-orbit coupling constant Potential energy surfaces Complete active space self-consistent field calculation (CASSCF)

16. SECURITY CLASSIFICATION OF:			17. LIMITATION OF ABSTRACT	18. NUMBER OF PAGES	19a. NAME OF RESPONSIBLE PERSON
a. REPORT	b. ABSTRACT	c. THIS PAGE			Rainer A. Dressler
UNCL	UNCL	UNCL	UNL	14	19B. TELEPHONE NUMBER (Include area code)

THE JOURNAL OF CHEMICAL PHYSICS 128, 234306 (2008)

On the *R*-dependence of the spin-orbit coupling constant: Potential energy functions of Xe_2^+ by high-resolution photoelectron spectroscopy and *ab initio* quantum chemistry

O. Zehnder,[1] R. Mastalerz,[1] M. Reiher,[1,a)] F. Merkt,[1,b)] and R. A. Dressler[2,c)]
[1]*Laboratorium für Physikalische Chemie, ETH Zurich, 8093 Zurich, Switzerland*
[2]*Air Force Research Laboratory, Space Vehicles Directorate, Hanscom AFB, Massachusetts 01731-3010, USA*

(Received 18 March 2008; accepted 5 May 2008; published online 19 June 2008)

The pulsed-field-ionization zero-kinetic-energy photoelectron spectrum of Xe_2 has been measured between 97 350 and 108 200 cm^{-1}, following resonant two-photon excitation via selected vibrational levels of the $C\,0_u^+$ Rydberg state of Xe_2. Transitions to three of the six low-lying electronic states of Xe_2^+ could be observed. Whereas extensive vibrational progressions were observed for the transitions to the $I(3/2g)$ and $I(3/2u)$ states, only the lowest vibrational levels of the $II(1/2u)$ state could be detected. Assignments of the vibrational quantum numbers were derived from the analysis of the isotopic shifts and from the modeling of the potential energy curves. Adiabatic ionization energies, dissociation energies, and vibrational constants are reported for the $I(3/2g)$ and the $I(3/2u)$ states. Multireference configurational interaction and complete active space self-consistent field calculations have been performed to investigate the dependence of the spin-orbit coupling constant on the internuclear distance. The energies of vibrational levels, measured presently and in a previous investigation (Rupper *et al.*, J. Chem. Phys. **121**, 8279 (2004)), were used to determine the potential energy functions of the six low-lying electronic states of Xe_2^+ using a global model that includes the long-range interaction and treats, for the first time, the spin-orbit interaction as dependent on the internuclear separation. © *2008 American Institute of Physics*. [DOI: 10.1063/1.2937133]

I. INTRODUCTION

The rare gas dimer ions represent model systems to study ion-atom collisions. They are a source of absorption losses in excimer and ion lasers[1–3] and are encountered in high-pressure lamps and plasmas.[4] The potential energy curves of rare gas dimer ions are the key to understanding their decay and fragmentation dynamics,[5–11] and are required to model highly electronically excited states of the neutral dimers by multichannel quantum defect theory. Detailed knowledge of the potential energy functions of these ions is also important for a fundamental understanding of the chemical binding and the fragmentation dynamics of larger rare gas cluster ions,[12–22] and is a prerequisite for the calculation of charge-exchange[23] and differential scattering cross sections[24] that are necessary to model the effects of rare gas plasmas associated with electric space propulsion thrusters.

The homonuclear rare gas dimer ions Rg_2^+ (Rg=Ne, Ar, Kr, Xe, and Rn) possess six low-lying, closely spaced electronic states. At short internuclear distances, these states can be labeled using Mulliken's notation[25] as $A\,^2\Sigma_{1/2u}^+$, $B\,^2\Pi_{\Omega g}$, $C\,^2\Pi_{\Omega u}$ and $D\,^2\Sigma_{1/2g}^+$ (Ω=1/2,3/2). At large internuclear distances, the spin-orbit interaction mixes Σ and Π electronic states of the same value of Ω and same g/u symmetry. The appropriate labeling then is $I(1/2u)$, $I(3/2g)$, $I(3/2u)$, $I(1/2g)$, $II(1/2u)$, and $II(1/2g)$, where the value of Ω and the g/u symmetry are given in parentheses and the labels I and II designate states correlating with the first $Rg(^1S_0)+Rg^+(^2P_{3/2})$ and second $Rg(^1S_0)+Rg^+(^2P_{1/2})$ dissociation limits, respectively.

Whereas early investigations were primarily concerned with the qualitative features of the electronic structure of the rare gas dimer ions,[25] recent experimental and theoretical studies have provided quantitative information on the potential energy curves of several electronic states of Ne_2^+,[26,27] Ar_2^+,[27–29] Kr_2^+,[27,30] and Xe_2^+.[31,32]

Most experimental data on the low-lying electronic states of Xe_2^+ have been obtained by He I,[33,34] threshold[35–38] and pulsed-field-ionization zero-kinetic-energy.[32,39] (PFI-ZEKE) photoelectron spectroscopy, and electron impact ionization.[11] Previous experimental studies of the photoelectron spectrum of Xe_2 have provided data on the $I(1/2u)\leftarrow X\,0_g^+$, $I(3/2g)\leftarrow X\,0_g^+$ and $II(1/2u)\leftarrow X\,0_g^+$ photoionizing transitions.[32,36–39] The spectroscopic data available on the $I(3/2u)\leftarrow X\,0_g^+$, $I(1/2g)\leftarrow X\,0_g^+$ and $II(1/2g)\leftarrow X\,0_g^+$ transitions are much less extensive. The vibrational assignment of the $I(1/2u)$, $I(3/2g)$, and $I(3/2u)$ states are unambiguous. Lu *et al.*[38] suggested the origin of the $II(1/2u)$ state to be located at 107 109 cm^{-1} above the neutral ground state, while Rupper *et al.* found its origin to be located at 107 157.7 cm^{-1}. Tonkyn and White[39] and Rupper *et al.*[32] have determined three vibrational levels (v^+=0,1,2) of the

a)Electronic mail: markus.reiher@phys.chem.ethz.ch.
b)Electronic mail: merkt@phys.chem.ethz.ch.
c)Present address: Spectral Sciences, Inc., 4 Fourth Av., Burlington, MA 01803-3804, USA.

$I(3/2u)$ state by PFI-ZEKE photoelectron spectroscopy using single-photon excitation from the $X\,0_g^+$ ground neutral state of Xe_2. The $I(1/2g)$ state has not been observed experimentally so far and is reported to be either repulsive[40,41] or weakly bound.[13,31,32,42] Lu *et al.*[38] attributed a line at $\sim 107\,715\ cm^{-1}$ in their threshold photoelectron spectrum to the origin of the $II(1/2g)$ state. Rupper *et al.*[32] also observed an isolated line at $108\,132.3\ cm^{-1}$ in their spectrum, which they tentatively attributed to the $II(1/2g)$ $(v^+=0) \leftarrow X\,0_g^+$ transition. When combined with the results of semiempirical[25] and *ab initio* quantum chemical[31,40–43] calculations, these experimental results provide a qualitative understanding of the relative role of short-range, long-range, and spin-orbit interactions and a qualitative description of the strengths and lengths of the bonds in all six low-lying electronic states of Xe_2^+. However, despite the considerable experimental and theoretical efforts that have been invested to derive accurate potential energy functions for these states, several assignments remain controversial. Moreover, all theoretical and experimental determinations of the potential energy functions of the six lowest electronic states of Xe_2^+ have been based so far on the assumption that the spin-orbit coupling constant is independent of the internuclear separation R. This assumption was first made and justified by Cohen and Schneider[44] for Ne_2^+, but has never been rigorously tested for the heavier rare gas dimers.

The main objectives of the present work were (1) to obtain a complete set of experimental data on the vibronic energy level structure of Xe_2^+, (2) to remove all persisting ambiguities in the spectral assignments, and (3) to identify, and if possible to quantify, the effects of a potential dependence of the spin-orbit coupling constant on the internuclear distance by combining the results of high-resolution photoelectron spectroscopy with those of *ab initio* quantum chemistry.

To this end, a new investigation of the $I(3/2g)$, $I(3/2u)$, and $II(1/2u)$ states of Xe_2^+ by resonance-enhanced two-photon ionization via selected vibrational levels of the $C\,0_u^+$ intermediate state of Xe_2 was carried out. Xe_2^+ was selected because the very large spin-orbit interaction seemed ideally suited for the detection of a potential R-dependence of the spin-orbit coupling constant. This experimental study was accompanied by an *ab initio* quantum chemical study of the R-dependence of the spin-orbit coupling constant.

A $(1+1')$ two-photon excitation scheme via selected vibrational levels of the $C\,0_u^+$ Rydberg state of Xe_2 located in the vicinity of the $Xe^*([5p]^5 6s'[1/2]_1)+Xe(^1S_0)$ dissociation limit has been used to access the ionic levels. This species-selective excitation scheme enables one to avoid undesirable contributions to the spectra originating from the ionization of free xenon atoms or of large clusters which completely obscure several regions of the single-photon PFI-ZEKE photoelectron spectrum.[32] Moreover, selecting different vibrational levels of the $C0_u^+$ intermediate state enables one to access different vibrational levels of the cation. Transitions to the vibrational levels up to $v^+=52$ of the $I(3/2g)$ state and up to $v^+=22$ of the $I(3/2u)$ state have been observed and unambiguously assigned. The assignment of the $II(1/2u)$ state proposed by Rupper *et al.*[32] was confirmed in an analysis of the isotopic shifts. In the range between 97 800 and 97 900 cm^{-1}, several features could be observed in the spectra which may be members of the $I(1/2g) \leftarrow X\,0_g^+$ progression. However, an unambiguous assignment was not possible. No transitions to the $II(1/2g)$ state were observed following resonant two-photon excitation via the $C\,0_u^+$ Rydberg state.

II. COMPUTATIONAL DETAILS

The nuclear charge of xenon $(Z=54)$ requires scalar and spin-orbit relativistic effects to be taken into consideration in all quantum chemical calculations on Xe_2^+. Therefore, the scalar-relativistic second-order[45] and eighth-order (optimum parametrization)[46] Douglas–Kroll–Hess one-electron Hamiltonians[47–49] were employed in all-electron calculations. Spin-orbit coupling was considered as a perturbation. For the approximation of the total electronic wave function, several configuration-interaction-type wave functions were investigated.

The first model chosen was a minimal multiconfiguration self-consistent field wave function as provided by the complete active space self-consistent field (CASSCF) method.[50] An active space of 6 orbitals (corresponding to the $5p$ shell of Xe) with 11 electrons was chosen to represent the lowest *gerade* and *ungerade* electronic states with either Σ or Π symmetry. The dynamic electron correlation was estimated in a multiconfiguration second-order perturbation-theory[51] (CASPT2) approach involving the $4d$, $5s$, and $5p$ shell of Xe. State-average CASSCF, state-average CASPT2 and state-interaction spin-orbit[52] calculations were carried out with the MOLCAS electronic structure package[53] using the arbitrary-order DKH module.[54,55] In all CASSCF/CASPT2 and spin-orbit state-interaction calculations the atomic natural orbital relativistic core correlated (ANO-RCC) basis set of Roos *et al.* of the following size $(22s/19p/13d/5f/3g)/[10s/9p/8d/5f/3g]$ was employed, where the figures in parentheses refer to the exponents of the basis set and those in brackets represent the contracted basis functions.[56] Atomic mean-field integrals[57,58] (AMFIs) and the electronic energy obtained from the CASPT2 calculations were used to set up the spin-orbit matrix for the state-interaction procedure in order to obtain the spin-orbit coupled states.

To assess the accuracy of the minimal CASSCF model, we performed second-order Douglas–Kroll–Hess multireference configuration interaction calculations with single and double excitations[59] (MRCISD) with the MOLPRO program suite[60] and the arbitrary-order DKH module,[54] explicitly correlating 35 electrons (i.e., the $4d$, $5s$, and $5p$ shell of Xe). An estimate of the contribution of higher-order excitations to the electronic energy was made by taking the Davidson correction into account.[61] In the MRCI calculations we also employed the ANO-RCC basis set of Roos *et al.*,[56] but in a fully decontracted manner. All calculations were carried out for internuclear distances ranging from 4.0 to 14.0 a.u. In order to estimate the effect of core electron correlation on spectroscopic parameters we additionally performed Davidson-corrected MRCISD calculations correlating solely the va-

TABLE I. Computational details, equilibrium bond distances R_e, and harmonic vibrational constants ω_e of the $^2\Sigma_u^+$ and $I(1/2u)$ states. The all-electron MRCI and CASPT2 data were obtained with a second-order scalar-relativistic Douglas–Kroll–Hess (DKH2) Hamiltonian. The symbol Q denotes Davidson-corrected MRCI results. The abbreviation SOC indicates the type of integrals used to construct the spin-orbit matrix for the perturbative state-interaction approach (indicated as "+SO" in the denomination of the method). For further information on the methods see text. The coupled-cluster CCSD-T data taken from Ref. 31 had been obtained for a restricted Hartree–Fock (HF) reference wave function with a distance-independent spin-orbit coupling constant according to Cohen and Schneider (denoted as "semiempirical" in the table). In Ref. 31, the HF orbitals were obtained with the core electrons replaced by an effective core potential (ECP) and including a core polarization potential.

Method	MRCI+Q(DKH2)	CASPT2(DKH2)	MRCI+Q(DKH2)	HF-CCSD-T(ECP)[a]
No. of correlated e^-	35	35	15	35
No. of configurations	137 808 730	6	11 162 040	...
basis set	$(22s/19p/13d/5f/3g)$	$[10s/9p/8d/5f/3g]$	$(22s/19p/13d/5f/3g)$	$[6s/6p/6d/6f/2g]$
$^2\Sigma_u^+$: R_e (pm)	307.5	303.4	310.6	...
$^2\Sigma_u^+$: ω_e (cm^{-1})	136.1	134.0	124.3	...
	MRCI+Q(DKH2+SO)	CASPT2(DKH2+SO)	MRCI+Q(DKH2+SO)	HF-CCSD-T(ECP+SO)[a]
Plus SOC	Breit–Pauli	AMFI	Breit–Pauli	Semiempirical
SOC basis set	$(22s/19p/13d)$	$[10s/9p/8d/5f/3g]$	$(22s/19p/13d)$	...
$I(1/2u)$: R_e (pm)	311.5	306.5	315.8	311.4
$I(1/2u)$: ω_e (cm^{-1})	124.5	124.5	112.6	123.2

[a]Reference 31.

lence region (the $5s$ and $5p$ shell) of Xe (i.e., correlating only 15 electrons). The spin-orbit coupled electronic states were obtained in a state-interaction approach, by diagonalizing the matrix representation of the electronic Hamiltonian and the spin-orbit Hamiltonian in a basis of the eigenfunctions of the electronic Hamiltonian. The Breit–Pauli Hamiltonian was used to generate the spin-orbit matrix elements for the internal configurations. For external configurations an effective mean-field Fock operator was employed.[62] The spin-orbit matrix was constructed in a smaller $(22s/19p/13d)$ basis set, but the corresponding diagonal elements were shifted in energy to match the Davidson-corrected MRCI energies. An overview of selected spectroscopic parameters of the $A\ ^2\Sigma_u^+$ and $I(1/2u)$ states and the approximations involved in the quantum chemical calculations is given in Table I.

The Davidson-corrected MRCI model (MRCI+Q) with 35 correlated electrons features the best agreement with the coupled-cluster data provided by Paidarová and Gadéa.[31] The equilibrium bond distance and the harmonic vibrational constant are remarkably well reproduced. The CASPT2 calculation shows larger deviations when compared to Ref. 31. The equilibrium bond distance R_e is underestimated by about 4 pm in the CASPT2+SO calculations. It is overestimated by the same amount in the case of the 15-electron MRCI $+Q+$SO results. The 15-electron MRCI$+Q$ wave function is not a good approximation to the 35-electron MRCI$+Q$ model since core correlation needs to be taken into account explicitly.

Concerning the DKH order we note that the equilibrium bond lengths of the $^2\Sigma_u^+$ ground state changes by less than 0.5 pm when switching from the DKH2 to the DKH8 Hamiltonian in the CASPT2 calculations. Hence, this effect can be neglected and the second-order Hamiltonian DKH2 is sufficiently reliable.

III. EXPERIMENT

A $(1+1')$ resonance-enhanced two-photon excitation scheme was used to excite the lowest electronic states of Xe_2^+ via selected vibrational levels of the $C\ 0_u^+$ Rydberg state of Xe_2 located just below the $Xe^*([5p]^5 6s'[1/2]_1)+Xe(^1S_0)$ dissociation limit. The vibrational levels of the $C\ 0_u^+$ Rydberg state were chosen as intermediate levels because they are long lived and have been well characterized.[63,64]

The experimental setup used in the present study has been described in Refs. 65–67 and consists of a source of coherent, tunable vacuum ultraviolet (VUV) radiation and an electron/ion time-of-flight (TOF) mass spectrometer.

The laser system consists of three dye lasers pumped by the doubled and tripled output of a Nd:YAG (yttrium aluminum garnet) laser at a repetition rate of $16\frac{2}{3}$ Hz. The first two dye lasers were used to generate tunable VUV radiation by two-photon resonance-enhanced four-wave mixing in krypton. The output of the first dye laser was tripled using two successive β-barium borate (BBO) crystals and kept fixed so as to correspond to the $4p^5 5p[1/2]_0 \leftarrow 4p^6(^1S_0)$ two-photon resonance in krypton $[2\tilde{\nu}_1 = 94\,092.86\ \text{cm}^{-1}$ (Refs. 68 and 69)]. The fundamental output of the second dye laser was overlapped with that of the first one and focused into a gold-

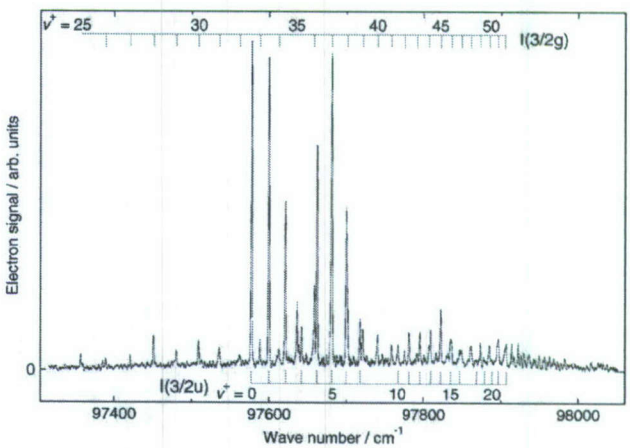

FIG. 1. PFI-ZEKE photoelectron spectrum of the $I(3/2g)$ and $I(3/2u)$ states of $^{132}Xe^{132}Xe^+$ recorded via the $v'=21$ vibrational level of the $C\ 0_u^+$ state.

TABLE II. Measured positions $\tilde{\nu}_{obs}$ and differences between measured and calculated positions ($\Delta\tilde{\nu}=\tilde{\nu}_{obs}-\tilde{\nu}_{calc}$) of the vibrational levels of the $I(3/2g)$ state of $^{131}Xe^{132}Xe^{+}$ relative to the $X\,0_g^+$ ($v''=0$) ground neutral state. The uncertainties include possible errors in the calibration and in the determination of the field-induced shift of the ionization thresholds. DL indicates the position of the $Xe^+(^2P_{3/2})+Xe(^1S_0)$ dissociation limit.

v^+	$\tilde{\nu}_{obs}$ (cm^{-1})	$\Delta\tilde{\nu}$ (cm^{-1})[a]	v^+	$\tilde{\nu}_{obs}$ (cm^{-1})	$\Delta\tilde{\nu}$ (cm^{-1})[a]	v^+	$\tilde{\nu}_{obs}$ (cm^{-1})	$\Delta\tilde{\nu}$ (cm^{-1})[a]
0	96 219.9(20)[b]	0.3	18		97 102.5	36	97 658.7(17)	−0.02
1	96 278.0(31)[b]	0.6	19		97 141.9	37	97 681.2(18)	0.7
2	96 334.7(36)[b]	0.6	20	97 179.3(11)[b]	−0.9	38	97 701.3(25)	−0.05
3	96 389.9(27)[b]	0.05	21	97 217.3(38)[b]	−0.2	39	97 721.3(17)	−0.01
4	96 445.0(22)[b]	0.4	22		97 253.8	40	97 740.0(20)	−0.4
5	96 497.7(39)[b]	−0.5	23		97 289.1	41	97 758.2(16)	−0.4
6	96 550.4(47)[b]	−0.5	24		97 323.4	42	97 775.4(16)	−0.5
7	96 602.2(26)[b]	−0.3	25	97 357.2(19)	0.5	43	97 792.0(16)	−0.4
8	96 652.4(38)[b]	−0.7	26	97 389.3(19)	0.2	44	97 807.2(17)	−0.9
9	96 701.7(11)[b]	−0.9	27	97 420.9(15)	0.5	45	97 822.6(16)	−0.4
10	96 750.1(18)[b]	−1.0	28	97 450.9(17)	0.2	46	97 836.3(29)	−0.8
11	96 797.0(17)[b]	−1.6	29	97 480.3(14)	0.2	47	97 849.3(25)	−1.1
12	96 844.2(25)[b]	−0.9	30	97 508.8(15)	0.3	48	97 861.5(28)	−1.4
13	96 889.4(11)[b]	−1.2	31	97 535.9(24)	0.01	49	97 873.7(17)	−1.1
14	96 935.0(10)[b]	0.01	32	97 562.5(22)	0.1	50	97 885.1(20)	−0.8
15	96 978.9(30)[b]	0.5	33	97 588.4(14)	0.5	51	97 895.9(10)	−0.5
16	97 021.2(28)[b]	0.4	34	97 612.9(18)	0.5	52	97 905.1(16)	−1.1
17	97 062.3(10)[b]	0.1	35	97 636.5(17)	0.5	DL	98 019.78	

[a]When the transitions could not be observed, the calculated positions are listed.
[b]Data from Rupper *et al.* (Ref. 32).

coated four-wave mixing cell with a slow constant flow of krypton at a pressure of ~16 mbars to generate the VUV radiation required to drive the $C\,0_u^+ \leftarrow X\,0_g^+$ transition of Xe_2. The VUV radiation was separated from the fundamental laser beams by a MgF_2 prism and directed toward the photoexcitation region where it intersected the probe gas beam and induced a transition to a selected vibrational level of the $C\,0_u^+$ state. The output of the third dye laser was used to access the electronic states of Xe_2^+ from the selected intermediate levels. The calibration of the fundamental wave number of the third dye laser was achieved by splitting off a small fraction of the laser beam and directing it toward an optogalvanic (OG) cell filled with neon or argon and, simultaneously, recording an étalon spectrum.

Xe_2 rare gas dimers were generated in a pulsed supersonic expansion of pure xenon (stagnation pressure of ~3.6 bars) through a pulsed solenoid valve (orifice diameter of 0.4 mm). Before entering the photoexcitation region the supersonic beam passed through a skimmer (orifice diameter of 1.0 mm). The supersonic beam crossed the laser beams at right angles.

PFI-ZEKE photoelectron spectra of Xe_2 were recorded by detecting the electrons produced by delayed pulsed field ionization of very high Rydberg states located below the vibronic states of Xe_2^+ using a sequence of two successive electric field pulses as a function of the wave number $\tilde{\nu}_3$ of the fundamental or doubled output of the third dye laser.

IV. RESULTS

A. The I(3/2*g*) and I(3/2*u*) states of Xe_2^+

PFI-ZEKE photoelectron spectra following single-photon excitation from the neutral ground state provided information only on the low vibrational levels of the $I(3/2g)$ and $I(3/2u)$ states of Xe_2^+ up to $v^+=21$ and $v^+=2$, respectively.[32] Close to the $Xe(^1S_0)+Xe^+(^2P_{3/2})$ dissociation

TABLE III. Measured positions $\tilde{\nu}_{obs}$ and differences between measured and calculated positions ($\Delta\tilde{\nu}=\tilde{\nu}_{obs}-\tilde{\nu}_{calc}$) of the vibrational levels of the $I(3/2u)$ state of $^{131}Xe^{132}Xe^{+}$ relative to the $X\,0_g^+$ ($v''=0$) ground neutral state. The uncertainties include possible errors in the calibration and in the determination of the field-induced shift of the ionization thresholds. DL indicates the position of the $Xe^+(^2P_{3/2})+Xe(^1S_0)$ dissociation limit.

v^+	$\tilde{\nu}_{obs}$ (cm^{-1})	$\Delta\tilde{\nu}$ (cm^{-1})[a]	v^+	$\tilde{\nu}_{obs}$ (cm^{-1})	$\Delta\tilde{\nu}$ (cm^{-1})[a]	v^+	$\tilde{\nu}_{obs}$ (cm^{-1})	$\Delta\tilde{\nu}$ (cm^{-1})[a]
0	97 577.6(15)	0.3	8		97 734.1	16	97 846.8(17)	−0.1
1	97 600.0(15)	0.5	9		97 750.5	17	97 858.1(16)	−0.2
2	97 621.4(16)	0.4	10	97 766.5(19)	0.3	18	97 868.8(15)	−0.3
3	97 642.2(12)	0.5	11	97 781.6(17)	0.4	19	97 879.0(24)	−0.3
4	97 662.2(16)	0.6	12	97 795.7(15)	0.1	20	97 888.8(16)	−0.3
5	97 681.2(19)	0.4	13	97 809.5(28)	0.2	21	97 896.9(13)	−1.4
6	97 699.8(23)	0.5	14	97 822.6(16)	0.2	22	97 907.0(12)	−0.1
7	97 717.6(15)	0.5	15	97 835.2(27)	0.2	DL	98 019.78	

[a]When the transitions could not be observed, the calculated positions are listed.

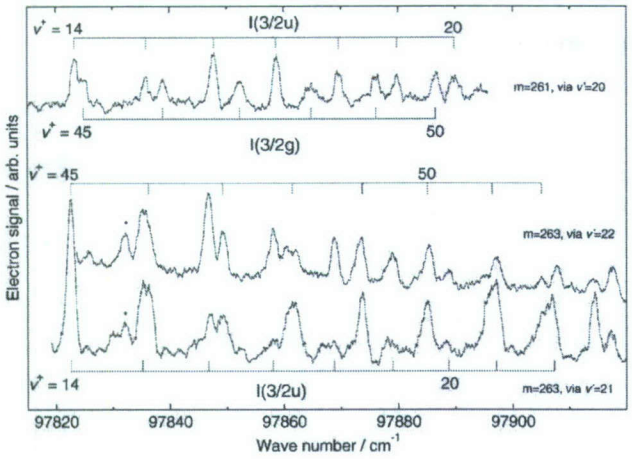

FIG. 2. PFI-ZEKE photoelectron spectra of the I(3/2*g*) and I(3/2*u*) states just below the $Xe^+(^2P_{3/2})+Xe(^1S_0)$ dissociation limit of $^{129}Xe^{132}Xe^+$ recorded via the $v'=20$ vibrational level of the $C\,0_u^+$ state (upper trace) and of $^{131}Xe^{132}Xe^+$ recorded via the $v'=21$ and 22 vibrational levels of the $C\,0_u^+$ state (lower traces).

limit the interpretation of the single-photon PFI-ZEKE photoelectron spectrum was complicated by atomic lines belonging to the Rydberg series converging to the $^2P_{3/2}$ dissociation limit of atomic xenon.[32] These undesirable atomic contributions could be avoided in the present work using a resonant—and thus species-selective—two-photon excitation sequence. Moreover, different regions of the ionic potential energy functions could be accessed by selecting different vibrational levels of the intermediate state.

The spectrum of the I(3/2*g*) and I(3/2*u*) states of $^{131}Xe^{132}Xe^+$ recorded via the $v'=21$ vibrational level of the $C\,0_u^+$ state is presented in Fig. 1. Long vibrational progressions were observed and assigned to levels as high as $v^+=52$ for the I(3/2*g*) state and $v^+=22$ for the I(3/2*u*) state. The unambiguous vibrational assignments were derived from an analysis of the isotopic shifts using the procedure described in Refs. 70 and 71. In the wave number region beyond 97 910 cm^{-1}, an unambiguous assignment of the spectral features could not be derived because of (1) the spectral congestion, (2) the weakness of most spectral features and (3) the irregularity of the intensity distribution partially caused by channel interactions with autoionizing Rydberg states.[72] These autoionizing states were independently observed in photoionization spectra recorded via the same intermediate vibrational levels of the $C\,0_u^+$ state (not shown here). Spectral lines in the photoelectron spectra observed in this region could correspond to vibrational levels of any of the four ionic states of Xe_2 associated with the $Xe^+(^2P_{3/2})+Xe(^1S_0)$ dissociation limit. The positions of the vibrational levels for the I(3/2*g*) and I(3/2*u*) states of $^{131}Xe^{132}Xe^+$ are summarized in Tables II and III.

The PFI-ZEKE photoelectron spectra of the I(3/2*g*) and I(3/2*u*) states of $^{129}Xe^{132}Xe^+$ and $^{131}Xe^{132}Xe^+$ between 97 820 and 98 000 cm^{-1} are compared in Fig. 2. The intensity distributions strongly depend on the selected vibrational level of the intermediate $C\,0_u^+$ state because of different Franck–Condon factors and channel interactions.[72] The top trace in Fig. 2 corresponds to the spectrum of the $^{129}Xe^{132}Xe$ isotopomer recorded via the $C\,0_u^+$ ($v'=20$) intermediate level whereas the bottom two traces correspond to spectra of $^{131}Xe^{132}Xe$ recorded through the $C\,0_u^+$ ($v'=21$ and 22) levels, as indicated. The line marked by an asterisk in the lower two traces of Fig. 2 could not be assigned to either the I(3/2*g*) or the I(3/2*u*) states of Xe_2^+. This line could correspond to a low vibrational level of the I(1/2*g*) state or to a high vibrational level ($v^+>110$) of the I(1/2*u*) state.

B. The II(1/2*u*) state of Xe_2^+

In our previous study of the lowest electronic states of Xe_2^+ following single-photon excitation from the $X\,0_g^+$ ground state of Xe_2, only transitions to the lowest twelve vibrational levels of the II(1/2*u*) state could be observed.[32] An unambiguous assignment of the absolute value of the vibrational quantum number was, however, hindered by the fact that the isotopic shifts were not large enough.

The isotope selectivity of the resonant two-photon excitation sequence used in the present investigation allowed the observation of the $II(1/2u)(v^+)\leftarrow X\,0_g^+$ progression for different isotopomers of Xe_2. The PFI-ZEKE photoelectron spectrum of the II(1/2*u*) state of $^{131}Xe^{132}Xe^+$ recorded via the $v'=21$ vibrational level of the $C\,0_u^+$ state of Xe_2 is displayed in the lower panel of Fig. 3 and the corresponding line positions are listed in Table IV. The decreasing background signal in the photoelectron signal between 107 100 and 107 350 cm^{-1} was caused by a strong electron signal close to the time gate of the background window in the TOF trace. These prompt electrons are mostly generated by processes where the laser beams hit metallic surfaces. The line marked by an asterisk corresponds to an impurity line. From the analysis of the isotopic shifts of the sixth line in the vibrational progression [see upper panels in Fig. 3 for a comparison of the assignments to $v^+=5$ (full lines) and to $v^+=6$ (dashed lines)], the vibrational assignment of the II(1/2*u*) state tentatively proposed by Rupper *et al.*[32] could be confirmed.

Unfortunately, the II(1/2*g*) state could not be observed from any of the selected vibrational levels of the intermediate $C\,0_u^+$ state and we are not able to confirm or refute the assignment of the single line observed in our previous study.[32]

C. Spectroscopic constants of the I(3/2*g*) and I(3/2*u*) states of Xe_2^+

Analyzing the vibrational progressions associated with the I(3/2*g*) and I(3/2*u*) states of $^{131}Xe^{132}Xe_2^+$ in terms of the standard expansion formula

$$\tilde{\nu}=E_i/hc+\omega_e^+(v^++1/2)-\omega_e x_e^+(v^++1/2)^2+\omega_e y_e^+(v^++1/2)^3-[\omega_e^+/2-\omega_e x_e^+/4+\omega_e y_e^+/8] \quad (1)$$

led to the set of adiabatic ionization energies E_i, harmonic (ω_e^+) and anharmonic ($\omega_e x_e^+$, $\omega_e y_e^+$, $\omega_e z_e^+$) vibrational constants summarized in Table V. Spectroscopic constants for the I(3/2*g*) state were derived using the transition wave numbers determined from the spectra shown in Figs. 1 and 2 and the positions of the lower vibrational levels reported by Rupper

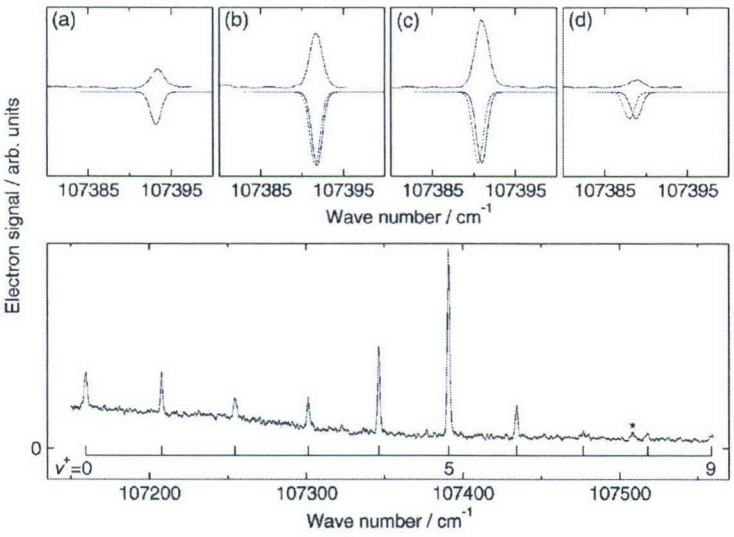

FIG. 3. Upper panels: upper traces: PFI-ZEKE photoelectron spectra of the II(1/2u) (v^+=5) state of different isotopomers of Xe_2^+ recorded via the v'=21 vibrational level of the $C\,0_u^+$ state. Lower inverted traces: Simulated spectra assuming that the ionic state has vibrational quantum number v^+=5 (full line) and v^+=6 (dashed line): (a) $^{129}Xe^{129}Xe$, (b) $^{129}Xe^{132}Xe$, (c) $^{132}Xe^{132}Xe$, and (d) $^{132}Xe^{136}Xe$. Lower panel: PFI-ZEKE photoelectron spectrum of the II(1/2u) state of $^{132}Xe^{132}Xe^+$ recorded via the v'=21 vibrational level of the $C\,0_u^+$ state. The line marked by an asterisk corresponds to an impurity line.

et al.[32] The constants of the I(3/2u) state were derived solely from the experimental data recorded in this work. In addition, values for the dissociation energies D_0^+ were determined from

$$D_0^+(Xe_2^+) = E_i(Xe, {}^2P_{J^+} \leftarrow {}^1S_0)/hc - E_i(Xe_2^+ \leftarrow Xe_2, X\,0_g^+)/hc + D_0(Xe_2, X\,0_g^+) \quad (2)$$

using the atomic ionization energies of 97 833.783 cm^{-1} corresponding to the formation of the $^2P_{3/2}$ state of Xe^+ (Ref. 73) and the dissociation energy D_0=186 cm^{-1} of the $X\,0_g^+$ ground state of Xe_2.[64] The spectroscopic constants summarized in Table V are consistent with the earlier results of Tonkyn *et al.*,[39] Lu *et al.*,[38] and Rupper *et al.*,[32] but represent a more complete set.

V. THE POTENTIAL ENERGY FUNCTIONS OF THE SIX LOW-LYING ELECTRONIC STATES OF Xe_2^+

A. Potential model

The semiempirical potential model first presented in Ref. 29 for the determination of the six lowest electronic potential functions of Ar_2^+ and later used for Kr_2^+ (Ref. 30) and Xe_2^+ (Ref. 32) was based, as all previous *ab initio* studies,[31,40–43] on the approximation of an R-independent spin-orbit coupling constant introduced by Cohen and Schneider.[44] The consequences of this approximation have never been quantified so far. Relativistic *ab initio* quantum chemical calculations (see Sec. II) allowed the investigation of the R-dependence of the spin-orbit coupling constant $a(R)$ by comparing the potential energy functions of the Π_u and Π_g states derived in scalar-relativistic calculations with those for the I(3/2u) and I(3/2g) states determined in relativistic calculations including also spin-orbit coupling. According to the spin-orbit interaction matrix presented in Table VI the potential energy functions of the $^2\Pi$ state and the $^2\Pi_{3/2}$ state differ by $a(R)/2$. Thus $a(R)$ can be determined at each internuclear separation for which both calculations have been performed by simple subtraction.

The upper sets of open squares and circles in Fig. 4 correspond to the values of $a(R)$ determined directly from the MRCI+Q (DKH2+SO) *ab initio* calculations (see column 1 in Table I). At large distances, the calculated spin-orbit coupling constants tend asymptotically to a value larger than the atomic value, both for the g and the u states. To

TABLE IV. Measured positions $\tilde{\nu}_{obs}$ and differences between measured and calculated positions ($\Delta\tilde{\nu}=\tilde{\nu}_{obs}-\tilde{\nu}_{calc}$) of the vibrational levels of the II(1/2u) and II(1/2g) states of $^{131}Xe^{132}Xe^+$ relative to the $X\,0_g^+$ (v''=0) ground neutral state. The uncertainties include possible errors in the calibration and in the determination of the field-induced shift of the ionization thresholds. DL indicates the position of the $Xe^+(^2P_{1/2})+Xe(^1S_0)$ dissociation limit.

v^+	$\tilde{\nu}_{obs}$ (cm^{-1})	$\Delta\tilde{\nu}$ (cm^{-1})	v^+	$\tilde{\nu}_{obs}$ (cm^{-1})	$\Delta\tilde{\nu}$ (cm^{-1})
0	107 159.6(23)	−1.6	8	107 517.8(29)	−1.2
1	107 207.7(17)	−1.4	9	107 558.7(38)	−1.0
2	107 254.5(24)	−1.6	10	107 603.2(29)[a]	3.8
3	107 301.2(19)	−1.0	11	107 643.9(16)[a]	5.7
4	107 346.4(17)	−1.0			
5	107 391.0(19)	−0.7		II(1/2g)	
6	107 434.3(19)	−0.7	0	108 132.3(13)[a,b]	
7	107 476.8(15)	−0.7	DL	108 556.71	

[a]Data from Rupper *et al.* (Ref. 32), incorrectly assigned to the $^{131}Xe^{132}Xe^+$ isotopomer. The corrected positions and deviations are 107 598.5(10) and −0.9 cm^{-1} for v^+=10 and 107 637.0(5) and −1.2 cm^{-1} for v^+=11, respectively.

[b]Data from Rupper *et al.* (Ref. 32). The values corresponds to $^{131.3}Xe_2^+$.

TABLE V. Adiabatic ionization energies E_i, dissociation energies D_0^+, and vibrational constants ω_e^+, $\omega_e x_e^+$, $\omega_e y_e^+$ of the I(3/2g) and I(3/2u) states of $^{131}Xe^{132}Xe^+$.

State	E_i (hc cm^{-1})	D_0^+ (cm^{-1})	ω_e^+ (cm^{-1})	$\omega_e x_e^+$ (cm^{-1})	$\omega_e y_e^+$ (cm^{-1})	Reference
I(3/2g)	96 220.7(15)	1799.1(15)	58.17(35)	0.456(26)	−0.001 98(73)[a]	This work[b–d]
	96 220.2(10)	1799.6(15)	58.61(27)	0.506(13)		32[b–d]
	96 226(4)	1793(5)	58.36(34)	0.484(15)		38[d,e]
	96 359(24)	1670(24)				34[d,e]
		⩾1220(5)[f]	⩾45[f]			39[d,e]
	96 327(40)	1694(40)				35[d,e]
	96 545(121)	1492(121)				33[d,e]
	96 343(40)	1815(40)	55.5(28)			81[e,g]
		1565(40)	55(4)			82[e,g]
	96 143	1876	58.74	0.508		31[e,h]
		1178	49.7	0.3		40[e,h]
I(3/2u)	97 577.6(15)	442.2(15)	23.19(54)	0.419(54)	0.002 7(15)	This work[b–d]
	97 576.6(10)	443.2(15)	21.89(40)			32[b–e]
	97 582(4)	437(5)				38[d,e]
	97 214(24)	807(24)				34[d,e]
	97 576(2)	442(2)	23.1	0.55		39[d,e]
	97 617(40)	403(40)				35[d,e]
		<403				33[d,e]
	97 512(40)	645(40)	33.0(17)			81[e,g]
		613(40)	33(4)			82[e,g]
	97 437	582	26.53	0.425		31[e,h]
		306	58.5	0.3		40[e,h]

[a] $\omega_e z_e^+ = -0.000\,026\,6(68)$ cm^{-1}.
[b] The uncertainties in E_i and D_0^+ include the full width at half maximum of the observed transitions and potential errors in the wave number calibration and in the determination of the field-induced shifts of the ionization thresholds.
[c] The uncertainty in the vibrational constants represent one standard deviation in the fit.
[d] Experimental values.
[e] Values correspond to a mixture of all isotopomers which is best represented by a fictive average isotopomer of Xe_2 with reduced mass μ=65.646 u.
[f] Tonkyn and White (Ref. 39) did not derive an absolute vibrational assignment of the I(3/2g) state.
[g] Semiempirical values using known spectroscopic data.
[h] Theoretical values.

correct for this artefact of the calculations, the curves were scaled by a factor of 0.933 for the u states and 0.928 for the g states so that the asymptotic value of $a(R)$ exactly corresponds to the spin-orbit splitting of the Xe^+ ^2P ground state. The scaled $a_{g/u}(R)$ values are also displayed in Fig. 4 (lower sets of open squares and circles). The spin-orbit coupling constant varies by about 10% over the range of internuclear distance relevant for the present study. Consequently, the R-dependence of the spin-orbit coupling constant must be included in a quantitative description of the potential energy functions of the six low-lying electronic states of Xe_2^+. We should note that also the minimal CASPT2 model (see column 2 in Table I) features a very similiar behavior of $a(R)$ although these $a(R)$ curves are below the asymptotic limit and would require a scaling factor that is slightly larger than 1. However, in view of the validation of the MRCI data in Sec. II, we consider only the MRCI+Q (DKH2+SO) data in the following.

TABLE VI. Spin-orbit interaction matrix in Hund's case (a) basis describing the coupling between the states of $^2\Sigma^+$ and $^2\Pi$ symmetry in the homonuclear rare gas dimer ions.

	$^2\Sigma_{1/2}^+$	$^2\Pi_{1/2}$	$^2\Pi_{3/2}$
$^2\Sigma_{1/2}^+$	$V_\Sigma(R)$	$-\frac{a(R)}{\sqrt{2}}$	
$^2\Pi_{1/2}$	$-\frac{a(R)}{\sqrt{2}}$	$V_\Pi(R)+\frac{a(R)}{2}$	
$^2\Pi_{3/2}$			$V_\Pi(R)-\frac{a(R)}{2}$

We found that the R-dependence of the scaled spin-orbit coupling constant $a(R)$ of the u and g states could be described almost perfectly by two rather simple analytical expressions,

$$a_u(R) = a_{\text{atom}} - a_{u,0}(1-(1-e^{-a_{u,1}(R-a_{u,2})})^2), \tag{3}$$

$$a_g(R) = a_{\text{atom}} + a_{g,0}e^{-a_{g,1}\cdot R^{a_{g,2}}}, \tag{4}$$

where

$$a_{\text{atom}} = a_{\text{Xe}} = \tfrac{2}{3}A_{\text{Xe}} = 7024.617 \text{ cm}^{-1}$$

($A_{\text{Xe}}=[E(Xe^+,{}^2P_{1/2})-E(Xe^+,{}^2P_{3/2})]/hc$).[74] Equation (3) is a Morse-type function and Eq. (4) falls exponentially at increasing R. The optimal parameters $a_{u,i}$ and $a_{g,i}$(i=0,1,2) are listed in the lower part of Table VII and the correspond-

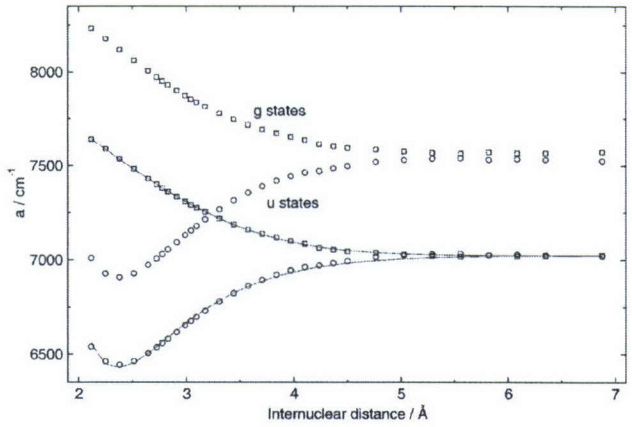

FIG. 4. R-dependent spin-orbit coupling constant $a(R)$ for the u (circles) and the g (squares) states derived from the comparison of the relativistic (including spin-orbit coupling) with the scalar-relativistic potential energy curves derived by MRCI+Q (DKH2) *ab initio* calculations (see column 1 in Table I) (upper pair of curves). The lower pair of curves are scaled such that the asymptotic value exactly corresponds to the spin-orbit splitting of the Xe^+ ^2P ground state. The full lines represent fits based on the expressions in Eqs. (3) and (4).

ing $a_u(R)$ and $a_g(R)$ curves are displayed as full lines in Fig. 4.

The effects of the spin-orbit interaction are treated using the same coupling matrix as proposed by Cohen and Schneider,[44] improved by the R-dependence of the spin-orbit coupling constant. The procedure consists of diagonalizing, at each value of the internuclear distance R, the spin-orbit interaction matrix given in Table VI. Because the spin-orbit operator only couples states of the same g/u symmetry, two distinct 3×3 matrices must be set up, one for the g states, the other for the u states. The spin-orbit interaction matrix is expressed in the basis set adequate for the short-range part of the potentials in which the quantum numbers Λ and Σ corresponding to the projection of the total electronic orbital and spin angular momenta onto the internuclear axis are good quantum numbers. Consequently, the electronic potential energies of the $^2\Sigma^+_{1/2}$, $^2\Pi_{1/2}$, and $^2\Pi_{3/2}$ states appear as diagonal elements. The spin-orbit operator is not only described by diagonal contributions of $\pm a(R)/2$ which induce a splitting of the $^2\Pi$ state into the two components $^2\Pi_{1/2}$ and $^2\Pi_{3/2}$, but also by off-diagonal elements $-a(R)/\sqrt{2}$ which couple states of the same value of Ω (the projection of the total angular momentum onto the internuclear axis), namely, the $^2\Sigma^+_{1/2}$ and $^2\Pi_{1/2}$ states.

The potential energy functions of the $^2\Sigma^+$ and $^2\Pi$ states under neglect of the spin-orbit interaction are expressed as

$$V_\Lambda(R) = A_\Lambda e^{-b_\Lambda R} - B_\Lambda e^{-b_\Lambda R/\beta_\Lambda} - \sum_{n=2}^{3} f_{2n}(R,b_\Lambda)\frac{C_{2n,\Lambda}}{R^{2n}} + V_{\text{diss}} \tag{5}$$

with $\Lambda=\Sigma,\Pi$. Because the $^2\Sigma^+_g$ state is only weakly bound, the second term in Eq. (5), which describes the chemical bond, is neglected for this state ($B_{\Sigma_g}=0$). V_{diss} is a constant used to relate the potential energies to the energy of the $X\,0^+_g$ ($v''=0$) ground neutral state and is defined as

$$V_{\text{diss}} = D_0(Xe_2, X\,0^+_g) + E_i(Xe, {}^2P_{3/2} \leftarrow {}^1S_0)/hc + \frac{a_{\text{atom}}}{2} \tag{6}$$

with $a_{\text{atom}}=a_{Xe}$. The value of $V_{\text{diss}}=101\,532.1$ cm^{-1} is obtained from the literature values $a_{\text{atom}}=\frac{2}{3}A_{Xe}=7024.617$ cm^{-1},[74] $E_i(Xe,{}^2P_{3/2})/hc=97\,833.783$ cm^{-1},[73] and $D_0(Xe_2,X\,0^+_g)=186$ cm^{-1}.[64]

Because the $^2\Sigma^+$ and $^2\Pi$ potential energy curves are correlated with the $Xe(^1S_0)+Xe^+(^2P)$ dissociation limit, the long-range behavior of these states is described in terms of the interaction between a neutral Xe atom and a Xe^+ ion. The long-range coefficients are equal for the u and the g states. Values for the C_4 and C_6 coefficients of Xe_2^+ were derived using the formalism described in the appendix of Ref. 67.

The potential energy functions $V_j(R)$ of the three u and the three g states were then calculated from the $V_{\Sigma_u}(R)$,

TABLE VII. Parameters of the interaction potentials of the lowest electronic states of Xe_2^+. The uncertainties represent 95% confidence intervals. Parameters given without uncertainties were held fixed.

	u states		g states	
	$^2\Sigma^+_u$	$^2\Pi_u$	$^2\Sigma^+_g$	$^2\Pi_g$
$R_{e,\Lambda}$ (Å)	3.077 89 ± 0.000 30	4.607 05 ± 0.000 51	7.5[a]	3.6960 ± 0.0022
$D_{e,\Lambda}$ (cm^{-1})	10 634.87 ± 0.62	470.967 ± 0.088		1772.25 ± 0.82
β_Λ	1.290 29 ± 0.000 47	4.0204 ± 0.0024		1.5162 ± 0.0024
b_Λ (Å^{-1})	2.151 50 ± 0.000 41	2.842 95 ± 0.000 53	1.1157 ± 0.0010	2.6963 ± 0.0019
$C_{4,\Lambda}$ (cm^{-1} Å^4)[a,b]	234 837	234 837	234 837	234 837
$C_{6,\Lambda}$ (cm^{-1} Å^6)[a,b]	2 331 794	1 167 755	2 331 794	1 167 755
A_Λ (cm^{-1})[c]	2.458×10^7	1.094×10^8	148 617	4.858×10^7
B_Λ (cm^{-1})[c]	6.764×10^6	1471		1.743×10^6
	$a_u(R)$		$a_g(R)$	
a_0 (cm^{-1})	597.2[a]		1084.5[a]	
a_1 (Å^{-1})	1.566[a]		0.086[a]	
a_2	2.359 Å[a]		2.500[a]	

[a]This parameter was kept constant during the fit.
[b]Using $1E_h=219\,474.6$ cm^{-1}, $1a_0=0.529\,177\,211$ Å. See Appendix in Ref. 67.
[c]Determined from the conditions $[dV_\Lambda(R)/dR]|_{R=R_{e,\Lambda}}=0$ and $V_\Lambda(R_{e,\Lambda})=V_{\text{diss}}-D_{e,\Lambda}$. See Appendix A in Ref. 29.

TABLE VIII. Measured positions $\tilde{\nu}_{obs}$ from Rupper *et al.* (Ref. 32) and differences between measured and calculated positions ($\Delta\tilde{\nu}=\tilde{\nu}_{obs}-\tilde{\nu}_{calc}$) of the vibrational levels of the I(1/2u) state of $^{131}Xe^{132}Xe^+$ relative to the $X\,0_g^+$ ($v''=0$) ground neutral state. The uncertainties include possible errors in the calibration and in the determination of the field-induced shift of the ionization thresholds. DL indicates the position of the $Xe^+(^2P_{3/2})+Xe(^1S_0)$ dissociation limit.

v^+	$\tilde{\nu}_{obs}$ (cm^{-1})	$\Delta\tilde{\nu}$ (cm^{-1})[a]	v^+	$\tilde{\nu}_{obs}$ (cm^{-1})	$\Delta\tilde{\nu}$ (cm^{-1})[a]	v^+	$\tilde{\nu}_{obs}$ (cm^{-1})	$\Delta\tilde{\nu}$ (cm^{-1})[a]
0	90 147.5(17)	3.5	21	92 512.3(30)	−2.3	42	94 455.2(12)	−1.2
1	90 269.8(20)	3.3	22	92 614.6(25)	−2.2	43	94 537.5(23)	−0.6
2	90 390.6(35)	2.6	23	92 715.8(30)	−2.3	44	94 618.4(15)	−0.4
3	90 510.5(17)	1.9	24	92 816.3(21)	−2.1	45	94 697.9(13)	−0.6
4	90 629.9(30)	1.6	25	92 915.4(14)	−2.3	46	94 777.2(23)	−0.06
5	90 748.1(14)	1.2	26	93 013.6(23)	−2.5	47	94 855.5(17)	0.5
6	90 866.0(13)	1.4	27	93 110.7(22)	−2.7	48	94 932.2(18)	0.4
7	90 982.5(11)	1.1	28	93 207.7(28)	−2.1	49	95 008.4(15)	0.8
8	91 097.4(19)	0.2	29	93 302.8(30)	−2.4	50	95 083.7(20)	1.3
9		91 212.0	30	93 396.9(13)	−2.7	51	95 157.2(19)	1.0
10	91 325.2(30)	−0.7	31	93 490.5(23)	−2.6	52	95 230.6(15)	1.5
11	91 438.1(24)	−0.7	32	93 583.3(17)	−2.3	53	95 303.3(16)	2.4
12	91 550.2(19)	−0.5	33	93 674.9(20)	−2.2	54	95 374.2(18)	2.4
13	91 660.6(28)	−1.1	34		93 767.6	55	95 443.9(18)	2.2
14	91 771.2(28)	−0.5	35	93 855.1(14)	−2.0	56	95 513.9(31)	3.3
15	91 879.5(22)	−1.2	36	93 944.0(14)	−1.7	57	95 581.7(20)	3.1
16	91 987.5(28)	−1.3	37	94 031.8(33)	−1.5	58	95 649.6(23)	4.1
17	92 094.1(28)	−1.8	38	94 118.2(26)	−1.7	59	95 715.1(17)	3.6
18		92 202.0	39	94 204.3(14)	−1.2	60	95 781.0(14)	4.5
19	92 305.7(30)	−1.5	40	94 288.7(14)	−1.4	61	95 845.5(37)	5.0
20	92 409.8(29)	−1.6	41	94 372.5(17)	−1.3	DL	98 019.78	

[a]When the transitions could not be observed, the calculated positions are listed.

$V_{\Pi_u}(R)$, $V_{\Sigma_g}(R)$, and $V_{\Pi_g}(R)$ potentials in a straightforward manner using the interaction matrix presented in Table VI. The calculated transition wave numbers were determined by numerically solving the radial Schrödinger equation

$$\left[-\frac{\hbar^2}{2\mu_i}\frac{d^2}{dR^2}+hcV_j(R)\right]\psi_{ijv}(R)=E_{ijv}\psi_{ijv}(R) \tag{7}$$

corresponding to the vibrational motion of the isotopomer with reduced mass μ_i in the potential $V_j(R)$ (see below). In Eq. (7), the indices i, j, and v designate the isotopomer, the electronic state, and the vibrational quantum number of the ion, respectively.

B. Fitting procedure

The parameters of the model potential energy functions [Eq. (5)] were derived from the experimental data in a nonlinear least-squares fitting procedure. The numerical procedure relied on a discrete variable representation (based on the Gauss–Chebyshev quadrature of the first kind[75–78]) on a grid with 801 equidistant grid points in the range of internuclear distances $R=2.0-10.0$ Å. In the fitting procedure, all parameters describing the long-range interaction were kept fixed at the values listed in Table VII.

1. u states

The u states are experimentally well characterized and the observed and unambiguously assigned vibrational bands [59 bands for the I(1/2u) state, 21 bands for the I(3/2u) state, and 12 bands for the II(1/2u) state] form a large data set with which the potential energy functions of the three electronic states of u symmetry can be determined. A total of eight parameters ($R_{e,\Lambda}$, $D_{e,\Lambda}$, β_Λ, b_Λ; $\Lambda=\Sigma,\Pi$) were refined in the fitting procedure. The coefficients of $a_u(R)$ were kept constant at the values derived from fitting the expression of Eq. (3) to the scaled spin-orbit coupling constant (see Fig. 4). We have also performed fits with 11 parameters [8 for the $^2\Sigma_u^+$ and $^2\Pi_u$ states, and 3 for $a_u(R)$]. The optimized values for $a_{u,0}$, $a_{u,1}$, and $a_{u,2}$ differed by less than 1% from the scaled *ab initio* values and no noticeable improvement of the quality of the fit resulted. The initial value for the equilibrium internuclear distance of the $^2\Sigma_u^+$ state was set to the *ab initio* value of $R_{e,\Sigma_u}=3.075$ Å derived from the MRCI+Q (DKH2) calculation (see first column of Table I). This value was supported by an independent measurement of the rotationally resolved photoelectron spectrum of the I(1/2u) state of Xe_2^+ (Ref. 79) and only changed slightly in the fit (see Table VII).

The calculated positions of the vibrational transitions of the I(1/2u), I(3/2u), and II(1/2u) states using the optimal parameter set summarized in Table VII are listed in Tables VIII, III, and IV where they are also compared with the experimental values. The normalized root-mean-square (rms) deviation of the best fit amounted to 1.04. This number implies that the quality of the fit is excellent.[80] The differences between observed and calculated vibrational positions were smaller than 5 cm^{-1} with the exception of the $v^+=11$ level of the II(1/2u) state for which the difference amounts to 5.7 cm^{-1}. Looking at the behavior of the discrepancies for the II(1/2u) state (see Table IV) one recognizes that these are much smaller for the vibrational transitions observed in

this work ($v^+=0-9$) than for those taken from Ref. 32 ($v^+=10-11$). A reanalysis of the data of Ref. 32 showed that the values for the vibrational levels $v^+=8-11$ of the II($1/2u$) state do not correspond to $^{131}Xe^{132}Xe$ but to another isotopomer of Xe_2^+, a conclusion which could only be drawn with the knowledge of the spectroscopic information derived in the present study.

2. g states

Of the three low-lying *gerade* electronic states only the I($3/2g$) state (48 observed vibrational levels) is well characterized experimentally. Because of the weakly bound nature of the $^2\Sigma_g^+$ state this state is only described by two parameters (R_{e,Σ_g} and b_{Σ_g}). The *ab initio* quantum chemical calculations suggest that the $^2\Sigma_g^+$ state is repulsive in the internuclear distances probed by this experiment (see Sec. II). Therefore, and somewhat arbitrarily, we set the value of the equilibrium internuclear distance of this state to the large value of $R_{e,\Sigma_g}=7.5$ Å and kept it fixed during the fitting procedure. Because of the lack of data on the I($1/2g$) and II($1/2g$) states the coefficients $a_{g,i}(R)$ ($i=0,1,2$) were held constant at the values derived from fitting the expression of Eq. (4) to the scaled *ab initio* $a_g(R)$ curve (see Fig. 4). A total of five parameters (1 for the $^2\Sigma_g^+$ and four for the $^2\Pi_g$ states) were refined for the g states.

The optimal parameter set for the description of the potential energy functions of the three g states is summarized in Table VII. The normalized rms deviation of the best fit amounted to 0.41. The low value of this deviation must be interpreted with some caution. Indeed, the experimental data set does not contain enough information on the I($1/2g$) and II($1/2g$) states. The adjustable parameter of the Σ curve suffices to place the position of the only observed level of the II($1/2g$) state at its observed position. The agreement between the calculated and observed positions of this level can thus not be considered as a proof of the assignment. The calculated positions of the vibrational levels of the I($3/2g$) and II($1/2g$) states are listed in Tables II and IV. A comparison of the calculated positions of the I($3/2g$) state with those from the experiment shows that the maximum absolute deviation amounted to -1.6 cm^{-1} for the $v^+=11$ level.

C. Potential energy functions

The potential energy functions of the three u and the three g states of Xe_2^+ derived from the $^2\Sigma_u^+$, $^2\Pi_u$, $^2\Sigma_g^+$, and $^2\Pi_u$ potential energy curves and the R-dependent spin-orbit coupling matrix displayed in Table VI are presented in Figs. 5 and 6. The dissociation energies and equilibrium internuclear distances of all six states are summarized and compared with values from other studies in Table IX.

1. Potential energy functions of the u states

The potential energy functions of the u states derived from the global fit are displayed as full lines in Fig. 5. Compared to the results of our previous study[32] (dashed lines in Fig. 5), the dissociation energies of the three u states are almost equal whereas the equilibrium internuclear distances have shifted to larger values. The increased bond lengths are

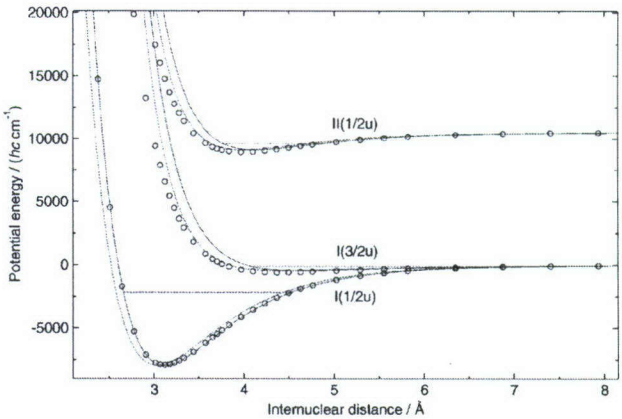

FIG. 5. Comparison of the potential energy functions of the I($1/2u$), I($3/2u$), and II($1/2u$) states of Xe_2^+ derived in this work (full line), in Ref. 32 (dashed line), and in Ref. 31 (circles). The dashed horizontal lines indicate for each state the positions of the highest observed vibrational level.

a result of a new rotationally resolved measurement of the low-lying electronic states of Xe_2^+.[79] The potential energy function of the I($1/2u$) state is in excellent agreement with that reported by Paidarová and Gadéa.[31] At internuclear distances smaller than ~4 Å the potential energy curves of the I($3/2u$) and II($1/2u$) states derived here are located higher in energy than those reported earlier[31,32] whereas the long-range behavior is almost identical. This discrepancy is likely to originate from the larger equilibrium internuclear distances of the $^2\Sigma_u^+$ and $^2\Pi_u$ states and from the R-dependent spin-orbit coupling constant. The effect of the R-dependence of a is further discussed in the Conclusions section.

2. Potential energy functions of the g states

The potential energy functions of the g states derived from the global fit are displayed as full lines in Fig. 6. The most remarkable feature in this figure is related to the potential energy function of the I($1/2g$) state which is only very weakly bound and gets its character mainly from the repulsive $^2\Sigma_g^+$ state. The low dissociation energy and the large

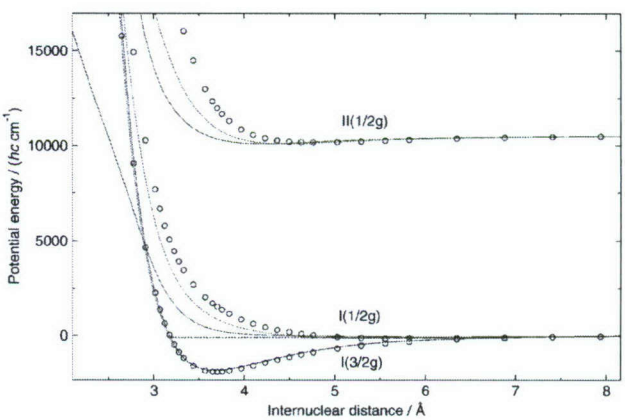

FIG. 6. Comparison of the potential energy functions of the I($1/2g$), I($3/2g$), and II($1/2g$) states of Xe_2^+ derived in this work (full line), in Ref. 32 (dashed line), and in Ref. 31 (circles). The dashed horizontal line indicates for the $I(3/2g)$ state the position of the highest observed vibrational level.

TABLE IX. Dissociation energies D_e and equilibrium internuclear distances R_e of the lowest electronic states of Xe_2^+ determined from the potential energy curves displayed in Figs. 5 and 6.

	I(1/2u)	I(3/2g)	I(3/2u)	I(1/2g)	II(1/2u)	II(1/2g)	Reference
D_e (cm^{-1})	7937.4	1829.5	453.9	72.9	1419.8	436.0	This work
	7932.7	1828.8	455.7	147.8	1430.2	436.1	32
	7904	1905	595	162	1602	368	31
	7178	1532	403	78	1371	242	42
	8691	1163	527	44	1690	307	13
	8646	1202	339	Repulsive	1686	Repulsive	40
	6372	968	242	Repulsive	968	61	41
R_e (Å)	3.118	3.683	4.632	6.096	4.130	4.199	This work
	3.034	3.674	4.390	5.437	3.985	4.448	32
	3.114	3.695	4.395	5.774	3.983	4.773	31
	3.17	3.19	4.76	6.35	4.13	5.29	42
	3.196	3.979	4.382	5.260	4.059	4.620	13
	3.18	3.91	4.00	Repulsive	3.97	Repulsive	40
	3.27	3.97	4.76	Repulsive	4.23	5.29	41

internuclear distance could explain why this state has not been observed in spectroscopic experiments so far. Whereas the dissociation energy and the equilibrium internuclear distance of the I(3/2g) state are comparable to those determined in our previous study the equilibrium internuclear distance of the II(1/2g) state has shifted to lower values. Because of the scarce experimental data on the g states, these potential energy functions strongly rely on the value of the equilibrium internuclear distance of the $^2\Sigma_g^+$ state obtained by *ab initio* MRCI+Q (DKH2+SO) quantum chemistry.

VI. CONCLUSIONS

The potential energy functions of the six low-lying electronic states of Xe_2^+ were derived, for the first time, by explicitly considering the R-dependence of the spin-orbit coupling constant as predicted by *ab initio* quantum chemistry. The effect of the R-dependence is best manifested by comparing the potential energy functions of the I(1/2u), I(3/2u), and II(1/2u) states calculated with an R-dependent spin-orbit coupling constant $a_u(R)$ with those calculated with an R-independent spin-orbit coupling constant $a=a_{\text{atom}}$ using the same Σ and Π potential energy curves (corresponding to the parameter set for the u states in Table VII). These potential energy curves and the corresponding energy differences are displayed in Fig. 7. The influence of the R-dependence gets significant at internuclear distances smaller than ~5 Å, where the deviation of the value of the spin-orbit-coupling constant from the atomic value becomes visible (see Fig. 4). Compared to the potential energy function of the I(3/2u) state calculated with $a=a_{\text{atom}}$, that calculated with $a_u(R)$ is shifted toward higher energies by ~50 cm^{-1} in the range of internuclear distances probed by the experiment, whereas that for the II(1/2u) state is shifted to lower energies by 60–110 cm^{-1}. The fact that the R-dependence of a has a larger effect on the I(3/2u) and II(1/2u) potential energy curves than on the I(1/2u) function can be explained by the strongly bound nature of the $^2\Sigma_u^+$ curve and the fact that, below 4.5 Å, this curve is separated from the Π curve by more than 3000 cm^{-1}.

The rms value of 1.04 for the best fit of the u states of Xe_2^+ suggests that the potential model and the R-dependence

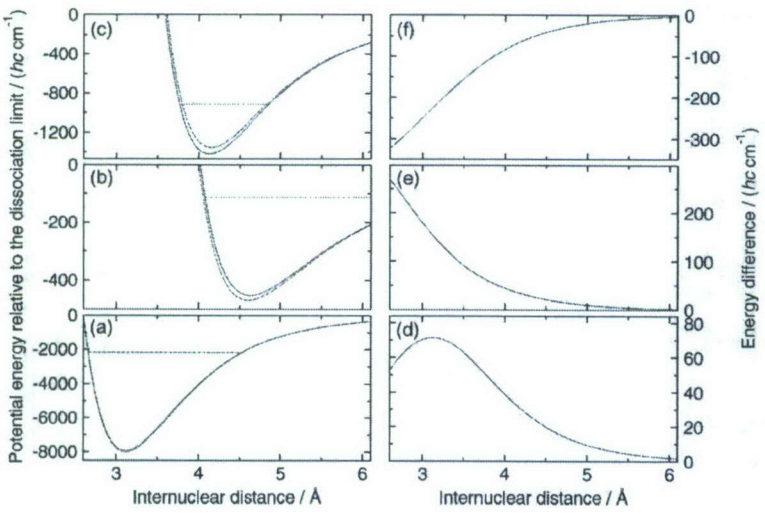

FIG. 7. Left panels: potential energy functions of the (a) I(1/2u), (b) I(3/2u), and (c) II(1/2u) states of Xe_2^+ calculated with R-dependent $a_u(R)$ (full lines) and R-independent $a=a_{\text{atom}}$ (dashed lines) using the same Σ and Π potential energy curves (parameter set for the u states in Table VII). The dashed horizontal lines indicate for each state the positions of the highest observed vibrational level. Right panels: energy difference of the two curves displayed in the left panels for the (d) I(1/2u), (e) I(3/2u), and (f) II(1/2u), states of Xe_2^+.

of the spin-orbit coupling constant are adequate to reproduce the data within the experimental uncertainties. The experimental data on the g states are much less extensive and the potential model appears to contain too many adjustable parameters leading to a rms value of 0.41 (see discussion in Sec. V). The quality of the potential energy functions of the six low-lying electronic states of Xe_2^+ could be improved by rotationally resolved spectroscopic investigations of these states which would also provide independent information on the internuclear separations. In addition, measurements of the two $(1/2\ g)$ states would be desirable. At present, the experimental data on the g states are too sparse for the determination of reliable potential energy functions.

The potential energy functions derived in this work reproduce the positions of all experimentally observed vibrational levels within their statistical uncertainties. This excellent agreement, which could not be reached in earlier analyses of the spectra of Kr_2^+ (Ref. 30) and Xe_2^+ (Ref. 32) using an R-independent spin-orbit coupling constant, is attributed to the inclusion, in the model, of the R-dependence of the spin-orbit coupling constant. The calculated R-dependence of the g and u functions can be well described by an exponentially decaying function [Eq. (4)] and a Morse-type function [Eq. (3)], respectively. Preliminary results on Ar_2^+ and Kr_2^+ suggest that these functions are also adequate to describe the R-dependence of the spin-orbit coupling constant in the other homonuclear rare gas dimer ions.

ACKNOWLEDGMENTS

We thank Professor Dr. Laura Gagliardi and Professor Dr. Roland Lindh for helpful discussions regarding the usage of the RASSI module in MOLCAS. R. A. Dressler is grateful for continued support by the Air Force Office of Scientific Research under task 2303EP02 (Program Manager: Michael Berman) and through a Windows on Europe grant. This work was supported financially by ETH Zurich and the Swiss National Science Foundation under Projects Nos. 200021-113479/1 (M.R.) and 200020-116245 (F.M.).

[1] *Excimer Lasers*, Topics in Applied Physics Vol. 30, 2nd ed., edited by C. K. Rhodes (Springer, Berlin, 1984).
[2] J. G. Eden, IEEE J. Sel. Top. Quantum Electron. **6**, 1051 (2000).
[3] J. J. Ewing, IEEE J. Sel. Top. Quantum Electron. **6**, 1061 (2000).
[4] *Vacuum Ultraviolet Spectroscopy*, edited by J. A. R. Samson and D. L. Ederer (Academic, San Diego, 2000).
[5] K. Stephan and T. D. Märk, Phys. Rev. A **32**, 1447 (1985).
[6] B. J. Whitaker, C. A. Woodward, P. J. Knowles, and A. J. Stace, J. Chem. Phys. **93**, 376 (1990).
[7] H. Yoshii, T. Hayaishi, T. Onuma, T. Aoto, Y. Morioka, and K. Ito, J. Chem. Phys. **117**, 1517 (2002).
[8] J. Fedor, R. Parajuli, S. Matt-Leubner, O. Echt, F. Hagelberg, K. Gluch, A. Stamatovic, M. Probst, P. Scheier, and T. D. Märk, Phys. Rev. Lett. **91**, 133401 (2003).
[9] J. Fedor, K. Głuch, R. Parajuli, S. Matt-Leubner, O. Echt, P. Scheier, and T. D. Märk, J. Chem. Phys. **121**, 7253 (2004).
[10] K. Gluch, J. Fedor, R. Parajuli, O. Echt, S. Matt-Leubner, and T. D. Märk, Eur. Phys. J. D **43**, 77 (2007).
[11] J. Fedor, O. Echt, K. Gluch, S. Matt-Leubner, P. Scheier, and T. D. Märk, Chem. Phys. Lett. **437**, 183 (2007).
[12] W. R. Wadt, Appl. Phys. Lett. **38**, 1030 (1981).
[13] M. Amarouche, G. Durand, and J. P. Malrieu, J. Chem. Phys. **88**, 1010 (1988).
[14] C. A. Woodward, B. J. Whitaker, P. J. Knowles, and A. J. Stace, J. Chem. Phys. **96**, 3666 (1992).
[15] A. B. Jones, P. R. Jukes, and A. J. Stace, J. Chem. Phys. **111**, 959 (1999).
[16] F. Y. Naumkin, Chem. Phys. **252**, 301 (2000).
[17] N. L. Doltsinis and P. J. Knowles, Chem. Phys. Lett. **325**, 648 (2000).
[18] D. Hrivňák and R. Kalus, Chem. Phys. **264**, 319 (2001).
[19] J. Galindez, F. Calvo, P. Paska, D. Hrivňák, R. Kalus, and F. X. Gadéa, Comput. Phys. Commun. **145**, 126 (2002).
[20] R. Kalus, I. Paidarová, D. Hrivňák, P. Paška, and F. X. Gadéa, Chem. Phys. **294**, 141 (2003).
[21] F. Calvo, J. Galindez, and F. X. Gadéa, Phys. Chem. Chem. Phys. **5**, 321 (2003).
[22] F. Calvo, F. X. Gadéa, A. Lombardi, and V. Aquilanti, J. Chem. Phys. **125**, 114307 (2006).
[23] J. S. Miller, S. H. Pullins, D. J. Levandier, Y. Chiu, and R. A. Dressler, J. Appl. Phys. **91**, 984 (2002).
[24] I. D. Boyd and R. A. Dressler, J. Appl. Phys. **92**, 1764 (2002).
[25] R. S. Mulliken, J. Chem. Phys. **52**, 5170 (1970).
[26] A. Carrington, D. I. Gammie, J. C. Page, A. M. Shaw, and J. M. Hutson, J. Chem. Phys. **116**, 3662 (2002).
[27] T.-K. Ha, P. Rupper, A. Wüest, and F. Merkt, Mol. Phys. **101**, 827 (2003).
[28] F. X. Gadéa and I. Paidarová, Chem. Phys. **209**, 281 (1996).
[29] A. Wüest and F. Merkt, J. Chem. Phys. **120**, 638 (2004).
[30] A. Wüest and F. Merkt, Mol. Phys. **103**, 1285 (2005).
[31] I. Paidarová and F. X. Gadéa, Chem. Phys. **274**, 1 (2001).
[32] P. Rupper, O. Zehnder, and F. Merkt, J. Chem. Phys. **121**, 8279 (2004).
[33] P. M. Dehmer and J. L. Dehmer, J. Chem. Phys. **68**, 3462 (1978).
[34] T. Pradeep, B. Niu, and D. A. Shirley, J. Chem. Phys. **98**, 5269 (1993).
[35] P. M. Dehmer, S. T. Pratt, and J. L. Dehmer, J. Phys. Chem. **91**, 2593 (1987).
[36] Y. Lu, T. Matsui, K. Tanaka, K. Ito, T. Hayaishi, and Y. Morioka, J. Phys. B **25**, 5101 (1992).
[37] R. I. Hall, Y. Lu, Y. Morioka, T. Matsui, T. Tanaka, H. Yoshii, T. Hayaishi, and K. Ito, J. Phys. B **28**, 2435 (1995).
[38] Y. Lu, Y. Morioka, T. Matsui, T. Tanaka, H. Yoshii, R. I. Hall, T. Hayaishi, and K. Ito, J. Chem. Phys. **102**, 1553 (1995).
[39] R. G. Tonkyn and M. G. White, J. Chem. Phys. **95**, 5582 (1991).
[40] H. H. Michels, R. H. Hobbs, and L. A. Wright, J. Chem. Phys. **69**, 5151 (1978).
[41] W. R. Wadt, J. Chem. Phys. **68**, 402 (1978).
[42] M. Daskalopoulou, H.-U. Böhmer, and S. D. Peyerimhoff, Z. Phys. D: At., Mol. Clusters **15**, 161 (1990).
[43] W. R. Wadt, J. Chem. Phys. **73**, 3915 (1980).
[44] J. S. Cohen and B. Schneider, J. Chem. Phys. **61**, 3230 (1974).
[45] A. Wolf, M. Reiher, and B. A. Hess, J. Chem. Phys. **117**, 9215 (2002).
[46] M. Reiher and A. Wolf, J. Chem. Phys. **121**, 2037 (2004).
[47] M. Douglas and N. M. Kroll, Ann. Phys. **82**, 89 (1974).
[48] B. A. Hess, Phys. Rev. A **33**, 3742 (1986).
[49] M. Reiher, Theor. Chem. Acc. **116**, 241 (2006).
[50] B. O. Roos, in *Advances in Chemical Physics; Ab Initio Methods in Quantum Chemistry*, edited by K. P. Lawley (Wiley, Chichester, England, 1987), Vol. 2, p. 399.
[51] K. Andersson, P.-Å Malmqvist, B. O. Roos, A. J. Sadlej, and K. J. Wolinski, J. Phys. Chem. **94**, 5483 (1990).
[52] B. O. Roos and P.-Å Malmqvist, Phys. Chem. Chem. Phys. **6**, 2919 (2004).
[53] G. Karlström, R. Lindh, P.-Å. Malmqvist, B. O. Roos, U. Ryde, V. Veryazov, P.-O. Widmark, M. Cossi, B. Schimmelpfennig, P. Neogrady, and L. Seijo, Comput. Mater. Sci. **28**, 222 (2003).
[54] M. Reiher and A. Wolf, J. Chem. Phys. **121**, 10945 (2004).
[55] M. Reiher and A. Wolf, Phys. Lett. A **360**, 603 (2007).
[56] B. O. Roos, R. Lindh, P.-Å Malmqvist, V. Veryazov, and P.-O. Widmark, J. Phys. Chem. A **108**, 2851 (2005).
[57] B. Schimmelpfennig, L. Maron, U. Wahlgren, C. Teichteil, H. Fagerli, and O. Gropen, Chem. Phys. Lett. **286**, 267 (1998).
[58] B. A. Hess, C. M. Marian, U. Wahlgren, and O. Gropen, Chem. Phys. Lett. **251**, 365 (1996).
[59] H.-J. Werner and P. J. Knowles, J. Chem. Phys. **89**, 5803 (1988).
[60] H.-J. Werner, P. J. Knowles, R. Lindh *et al.*, MOLPRO, Version 2002.6, a package of *ab initio* programs, 2002.
[61] S. R. Langhoff and E. R. Davidson, Int. J. Quantum Chem. **8**, 61 (1974).
[62] A. Berning, M. Schweizer, H.-J. Werner, P. J. Knowles, and P. Palmieri, Mol. Phys. **98**, 1823 (2000).
[63] R. H. Lipson, P. E. LaRocque, and B. P. Stoicheff, J. Chem. Phys. **82**, 4470 (1985).

[64] A. Wüest, U. Hollenstein, K. G. de Bruin, and F. Merkt, Can. J. Chem. **82**, 750 (2004).
[65] P. Rupper and F. Merkt, J. Chem. Phys. **117**, 4264 (2002).
[66] P. Rupper and F. Merkt, Rev. Sci. Instrum. **75**, 613 (2004).
[67] O. Zehnder and F. Merkt, J. Chem. Phys. **128**, 014306 (2008).
[68] V. Kaufman and C. J. Humphreys, J. Opt. Soc. Am. **59**, 1614 (1969).
[69] F. Brandi, W. Hogervorst, and W. Ubachs, J. Phys. B **35**, 1071 (2002).
[70] R. Signorell and F. Merkt, J. Chem. Phys. **109**, 9762 (1998).
[71] R. Signorell, U. Hollenstein, and F. Merkt, J. Chem. Phys. **114**, 9840 (2001).
[72] F. Merkt and T. P. Softley, Int. Rev. Phys. Chem. **12**, 205 (1993).
[73] F. Brandi, I. Velchev, W. Hogervorst, and W. Ubachs, Phys. Rev. A **64**, 032505 (2001).
[74] H. J. Wörner, M. Grütter, E. Vliegen, and F. Merkt, Phys. Rev. A **71**, 052504 (2005), see erratum in Phys. Rev. A **73**, 059904(E) (2006).
[75] R. Meyer, J. Chem. Phys. **52**, 2053 (1970).
[76] R. Meyer, J. Mol. Spectrosc. **76**, 266 (1979).
[77] J. T. Muckerman, Chem. Phys. Lett. **173**, 200 (1990).
[78] D. T. Colbert and W. H. Miller, J. Chem. Phys. **96**, 1982 (1992).
[79] K. Vasilatou, U. Hollenstein, and F. Merkt (unpublished).
[80] D. L. Albritton, A. L. Schmeltekopf, and R. N. Zare, in *Molecular Spectroscopy: Modern Research*, edited by K. N. Rao (Academic, New York, 1976), Vol. II, Chap. 1, pp. 1–67.
[81] E. C. M. Chen and E. S. Chen, Chem. Phys. Lett. **293**, 491 (1998).
[82] E. C. M. Chen, J. G. Dojahn, and W. E. Wentworth, J. Phys. Chem. A **101**, 3088 (1997).